Canadian Journal of Earth Sciences

Article

An experimental baseline for ice-till strain indicators

L.K. Zoet[a], **D.D. Hansen**[a], **N. Morgan-Witts**[a], **J. Menzies**[b], **P. Sobol**[a], **and N. Lord**[a]

[a]Department of Geoscience, University of Wisconsin-Madison, Madison, WI, USA; [b]Department of Earth Sciences, Brock University, St. Catharines, ON, Canada

Corresponding author: **L.K. Zoet** (email: lzoet@wisc.edu)

Abstract

Subglacial till can deform when overriding ice exerts shear traction at the ice–till interface. This deformation leaves a strain signature in the till, aligning grains in the direction of ice flow and producing a range of diagnostic microstructures. Constraining the conditions that produce these kinematic indicators is key to interpreting the myriad of features found in basal till deposits. Here, we used a cryogenic ring shear device with transparent sample chamber walls to slip a ring of temperate ice over a till bed from which we examined the strain signature in the till. We used cameras mounted to the side of the ring shear and bead strings inserted in the till to estimate the strain distribution within the till layer. Following the completion of the experiment, we extracted and analyzed anisotropy of magnetic susceptibility (AMS) samples and created thin sections of the till bed for microstructure analysis. We then compared the AMS and microstructures with the observed strain history to examine the relationship between kinematic indicators and strain in a setting where shear traction is supplied by ice. We found that AMS fabrics show a high degree of clustering in regions of high strain near the ice–till interface. In the uppermost zone of till, k_1 eigenvector azimuths are generally aligned with ice flow, and S_1 eigenvalues are high. However, S_1 eigenvalues and the alignment of the k_1 eigenvector with ice flow decrease nonlinearly with distance from the ice–till interface. There is a high occurrence of microshears in the zone of increased deformation.

Key words: till deformation, microstructures, anisotropy of magnetic susceptibility, glacial geology

1. Introduction

Many of the world's fastest moving glaciers slip atop till beds, and the mechanics active within these beds control glacier motion (Kamb 2001) and landform development (Clark 1993). Till deforms when the shear stress exerted by the overriding ice exceeds its yield strength, resulting in strain within the deforming zone that facilitates much of the overall glacier motion (Zoet and Iverson 2018, 2020; Hansen and Zoet 2022). Advances in our understanding of till dynamics (Tulaczyk et al. 2000*a*, 2000*b*; Damsgaard et al. 2013; Hansen and Zoet 2022) and coupling across the ice–till interface (Creyts and Schoof 2009; Zoet and Iverson 2018, 2020) emphasize that the physical properties of till—such as grain size, permeability, and bearing capacity—directly influence ice mass flux and therefore are central in affecting rates of sea-level rise. Furthermore, experimental (Hansen and Zoet 2022) and numerical (Damsgaard et al. 2020; Kasmalkar et al. 2021) investigations demonstrate that the mechanics of till deformation regulate subglacial sediment transport. This in turn affects rates and locations of aggradation and erosion at the ice–bed interface, as well as the formation mechanisms for myriad glacial landforms, including drumlins (Menzies et al. 1997, 2016; Woodard, et al. 2020; Zoet et al. 2021), flutes (Ives and Iverson 2019), grounding zone wedges (Bart and Tulaczyk 2020), and moraines (Colman et al. 2020).

Stored within the deposits of deforming till beds are kinematic indicators of past strain that convey flow conditions of paleo glaciers (Fig. 1). Investigation into subglacial till deposits spans decades, with researchers employing a variety of analytical and descriptive techniques (see Benn and Evans 2010, pp. 333–440 for a review). From these analyses, much has been learned about subglacial processes, which in certain cases upended prevailing theories in glaciology. Glacial geologists, for example, supposed that many fast-moving glaciers were underlain by deformable beds based on their observations of subglacial till well before it was an accepted fact in glaciology (Alley et al. 1986; see Boulton (1986) for a review on the topic). Research of subglacial till began largely through lithostratigraphic characterization, using tools such as grain size analysis, grain shape analysis, color, lithology, and clast fabric orientations, to describe and delineate till facies (Colgan et al. 2003). Over time, other methods to characterize till deformation gained prominence as well, including microstructural analyses (Menzies 2000; van der Meer et al. 2003; Menzies and Meer 2018) and anisotropy of magnetic susceptibility (AMS) (Iverson 2017). Through the combined application of these methods, as well as insights gleaned through experiments, numerical modeling, and geophysical surveys, a picture of the deforming bed has emerged of a heterogeneous mosaic of deforming and rigid sections (Anandakrishnan and Alley 1994; Piotrowski et al. 2001;

Fig. 1. Subglacial traction till that has been heavily strained beneath Mulajokull glacier in Iceland. Ice flow is from left to right along the white arrow. Ice axe shown for scale. Photo taken by L. Zoet.

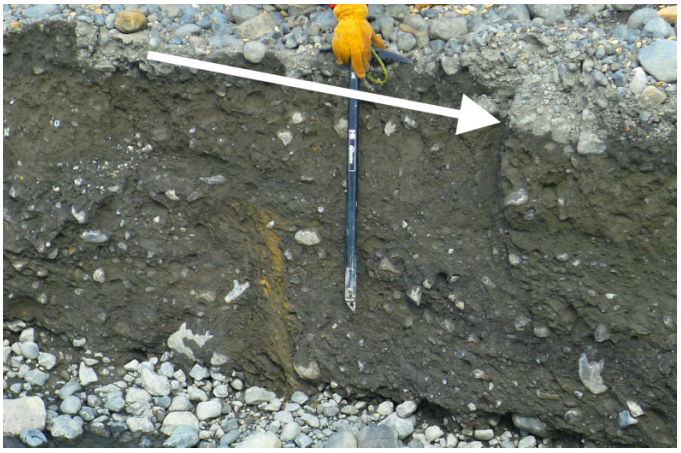

Shumway and Iverson 2009; Tylmann 2012; Kasmalkar et al. 2021).

The strain imposed by distinct stress conditions results in a range of fabrics that can help elucidate the kinematics of till deformation. Till squeezed into subglacial crevasses, for example, undergoes pure shear, resulting in girdled fabrics of elongated grains (Ankerstjerne et al. 2015). Alternatively, grains in a deforming zone near the ice–bed interface undergoing simple shear typically align with the direction of maximum strain (McCrackin et al. 2016). This orientation is a direct consequence of the Coulomb nature of the till (Iverson et al. 1998), since a viscous till model predicts Jeffery-style clast rotation (Hart et al. 2009), which is ill-suited to describe many observed characteristics of till deformation and grain alignment (Iverson et al. 2008). Elongated clast fabrics are therefore commonly used in kinematic analysis of subglacial tills to ascertain flow direction and serve as indicators of paleo strain orientation for certain conditions (e.g., matrix-supported clasts with sufficient strain) (McCrackin et al. 2016). Explicitly linking the azimuths of till strain and overall ice flow can be problematic when sufficient time has elapsed between the times of ice flow and measurement (Stanford and Mickelson 1985), when there is substantial local variation in ice direction and till strain (Shumway and Iverson 2009), or when macroscopic planes of shear are not horizontal (Iverson 2017).

AMS is an effective technique to infer the kinematics of till deformation as elongated magnetic grains arrange themselves systematically when deformed. The basis for AMS usage on tills was extensively developed in the laboratory using sediment ring shear devices (Iverson et al. 2008; Jacobson and Hooyer 2015), and the technique has been widely employed in the field to interpret landform development (Shumway and Iverson 2009; Gentoso et al. 2012; McCracken et al. 2016; Spagnolo et al. 2016; Ives and Iverson 2019). AMS measures the orientation of magnetic grains in till that align with the direction of maximum deformation once strain has become sufficiently large (Iverson et al. 2008). When till samples with shape-oriented magnetic minerals are collected and placed in an applied magnetic field, the resultant induced magnetic field can be measured to assess the strain history of the till.

Fig. 2. Classification of microstructures and matrix types identified in glaciated sediments (modified from Menzies 2000*a*, 2000*b*; Ravier 2014).

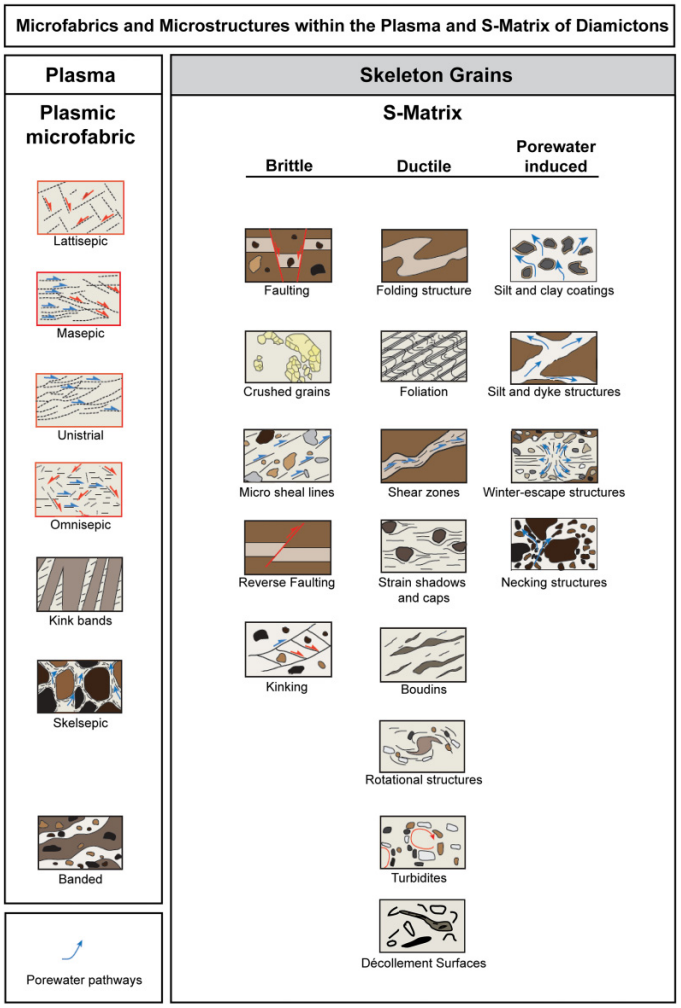

Additionally, the alignment of grains in general (beyond solely magnetic particles) can be observed microscopically to interpret till deformation. Till samples, collected with known orientations and prepared as thin sections, contain a plethora of microstructures when imaged with petrographic microscopes (Menzies and van der Meer 2018). These microstructures—which include grain bridges, shear structures, rotation (turbate or galaxy) structures, microshears, shear zones, among many others—represent the grain-scale accommodation of strain and therefore convey information regarding till strain direction and the local ice-flow azimuth of paleo glaciers and ice streams (Fig. 2). The microstructures of any sediment are composed of different components of variable sizes and shapes (such as clays, silts, and sand grains) distributed through a sediment in various random or ordered patterns. The components are distinguished from each other by their various crystalline, semicrystalline, or amorphous

Fig. 3. Ring shear apparatus. (A) Full load frame with the gear box that drives the upper platen, torque sensor that measures resistive torque to rotation, and vertical piston that supplies vertical overburden stress. (B) Close-up of the transparent sample chamber with till emplaced in the bottom of the sample chamber and ice atop the till. Cameras are used to monitor the movement of the till grains through the transparent side walls. (C) Schematic of the ring shear showing the Delrin teeth that grip the upper surface of the ice ring as the ice ring is spun over the till bed. Water is allowed to drain through a series of drainage ports, and water pressure is recorded with the pressure transducers. Figure from Hansen and Zoet (2022).

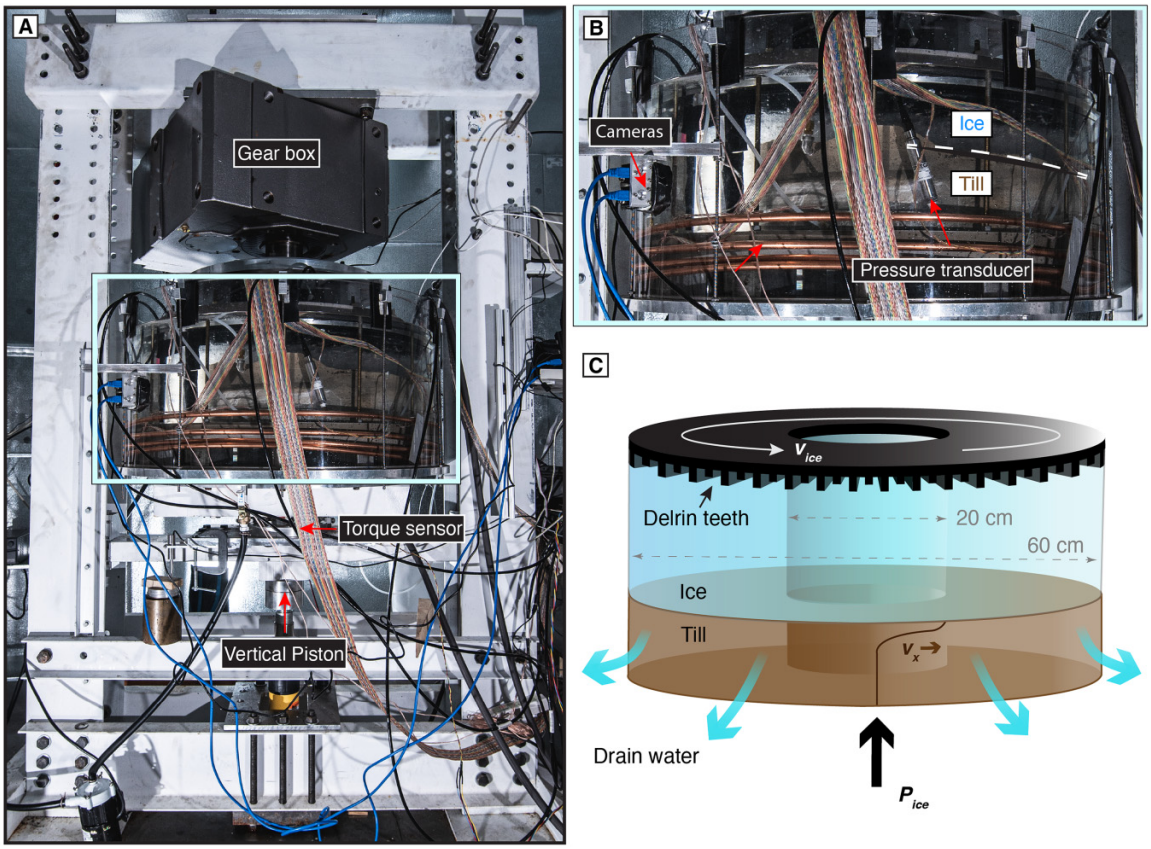

structures when observed under a microscope. The sedimentologist can observe a wide range of properties from such patterns and modifications produced during depositional and postdepositional processes. To assess sediment behavior at the microscale, it is essential to establish relationships between the macroscopic and microscopic properties and phenomena.

Numerous experimental studies have investigated AMS and microstructure patterns in deformed till using split-cell sediment ring shear devices (Müller and Schlüchter 2000; Hiemstra and Rijsdijk 2003; Larson et al. 2006; Thomason and Iverson 2006; Hooyer et al. 2008; Iverson et al. 2008). These devices shear an annulus of water-saturated sediment at a prescribed effective pressure and strain rate. In this configuration, sediment in the upper half of the ring overrides sediment in the lower half, while deformation is concentrated in a central shear band. Importantly, the total strain imposed on the till is precisely known at the conclusion of these experiments—meaning sediment extracted from the central deforming zone provides a baseline to calibrate AMS or microstructure measurements from the field, explore the veracity of competing grain rotation models, or conduct microstructure analysis from thin sections. From this body of work, it is evident that many features produced in the laboratory bear a close resemblance to those observed in the field. However, a key difference between these seminal laboratory studies and the natural setting is the presence of a viscous, temperate layer of ice that overlays the sediment and exerts the shear stress at the ice–till interface that drives till deformation.

Slip along the ice–till interface is complicated by the viscous coupling of ice to the till (Tulaczyk 1999; Zoet and Iverson 2018, 2020) and ongoing melt, which passes meltwater through the till or moves along the ice–till boundary in accordance with the hydropotential gradient. Stress is transferred across the ice–till interface and, if sufficiently large, will deform the underlying sediment (Zoet and Iverson 2020; Hansen and Zoet 2022). The total motion of the ice is then partitioned between till deformation and sliding along the ice–bed interface. How the direction of ice slippage directly translates into the strain azimuth preserved in the underlying till and how the coupling across the interface affects the microstructural deformation mechanisms in the deforming till remain open questions. Passage of meltwaters through the till may result in a spatially and temporally heterogeneous till yield strength and heterogeneous coupling of the

Fig. 4. Cumulative grain size distribution of Horicon till used in the experiments. The D_{50} grain size is 530 μm. Figure from Hansen and Zoet (2022).

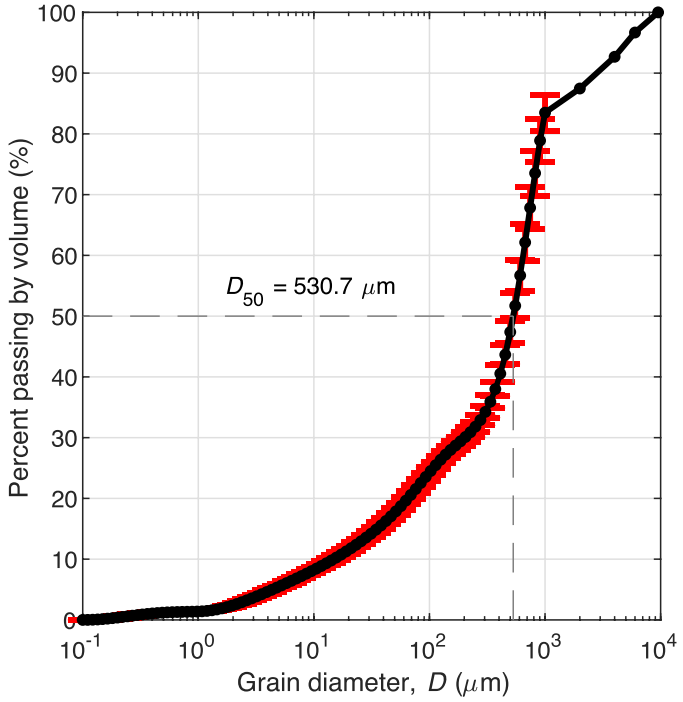

ice–bed interface, which could result in a variation in the deformation structures from those resolved in sediment-only shear devices.

With this study, we established a baseline to assess ice-induced deformation of an underlying till bed. Using a novel cryogenic ring shear device at UW-Madison with transparent sample chamber walls, we sheared temperate ice over a layer of subglacial till at prescribed slip rates and effective pressures. We then evaluated deformation in the till bed using four complementary techniques: (i) AMS, (ii) microstructural analysis, (iii) excavating passive strain markers in the bed, and (iv) computing displacement fields with digital image correlation (DIC) from a photographic time series of deforming till. Fabric analysis from AMS and microstructural observations were compared against the known depth-dependent deformation history of the till from the beads and DIC. We found that till deformation primarily localizes to a narrow zone near the ice–bed interface, and a clear link exists between AMS fabrics, thin section microstructures, and the amount of strain recorded in the till.

2. Methods

2.1. Ring shear experiment

We slid temperate ice over water-saturated till using a large-diameter, cryogenic ring shear device in the UW-Madison Surface Processes lab. The sample chamber of the ring shear was constructed from two concentric, transparent acrylic cylinders (outer diameter: 60 cm; inner diameter: 20 cm; height: 30 cm) mounted atop an aluminum base plate (Fig. 3). A hydraulic ram at the base of the device applied a vertical stress that compressed the till and ice, simulating the overburden stress of the glacier. Water pressure sensors, mounted to the external walls and ported to the interior of the sample chamber, measured porewater pressure. Effective pressure on the sediment was estimated by subtracting the average water pressure from the average imposed vertical stress over a given interval. The device is housed in a large walk-in freezer with temperature control of $\pm$ 1 °C, and the sample chamber was immersed in a propylene glycol/water bath, regulated by an external circulator with ~0.01 °C precision. These combined temperature controls kept the ice at its pressure melting point for the duration of the experiment. A toothed upper platen gripped the top of the ice ring and rotated at a prescribed rate, forcing the ice ring to slip over the bed. An 11 cm thick layer of subglacial till was placed in the base of the sample chamber, which was sourced from the late Wisconsinan Horicon Member of the Holy Hill Formation in Wisconsin, USA (Mickelson and Syverson 1997). The grain size distribution of the sediment was approximately fractal (Fig. 4), though clasts larger than 9.51 mm were removed prior to emplacement to prevent boundary effects (Head 1989). Two vertically stacked FLIR digital cameras mounted to the external perimeter of the glycol/water bath tracked motion in the till through the transparent walls (Fig. 3). Grain displacement vectors determined from DIC were summed to provide depth-dependent strain estimates of the sediment at the outer boundary of the sample chamber for areas of highly strained till (see Hansen and Zoet (2022) for details on DIC). Four strings of vertical beads were inserted in the till to serve as passive strain indicators, with two positioned at the outer boundary and two at the centerline, and were primarily used to estimate strain in the areas of relatively low strain. The ice ring was spun for ~9 days following the parameters listed in Table 1. We integrated all recorded strain at various layers within the till for comparison with AMS and microstructure results. The various velocities reported in Table 1 were used to infer the depth of deformation as reported in Hansen and Zoet (2022). All other experimental procedures are outlined in Hansen and Zoet (2022).

2.2. Anisotropy of magnetic susceptibility

Upon completion of the experiment, the ice ring was melted in place and water drained from the sample chamber. By melting the ice rather than extracting it, delicate deformation structures near the ice-bed interface were preserved. The bed was then allowed to further drain and air dry for ~24 h, at which point the till was still moist, indicating no desiccation occurred. In total, 94 cubic AMS sample boxes, sized 25 mm × 25 mm × 20 mm, were inserted for sample collection over five depth intervals. AMS sample boxes were pressed in the till as 4 × 5 grids with ~1 cm spacing (Fig. 5*a*). The orientation of each sample was recorded on each box and their positions were denoted by photographs of the box placement. Boxes were then gently removed with a spade, while scraping excess till aside, and then capped. Minimal disruption to the sample occurred through the emplacement and removal of the box, largely due to the lack of large obstructing clasts in

Table 1. Experimental metrics.

Velocity (m/yr)	Duration (h)	Displacement (m)	T_{sb} (m)	Strain, γ (-)
100	23.133	0.264	0.009	29.34
100	22.433	0.256	0.009	28.45
25	30.5	0.087	0.025	3.48
50	5.5	0.031	0.019	1.65
100	13.466	0.154	0.008	19.22
300	5.8	0.199	0.007	28.38
100	1.03	0.012	0.008	1.47
100	44.583	0.509	0.0165	30.85
300	44.5667	1.526	0.0157	97.21
100	13.5	0.1541	0.01	15.41
300	15.45	0.529	0.0087	60.82

Note: T_{sb} is the thickness of the shear band and γ is the strain.

Fig. 5. Sample collection following the completion of the experiment. (*a*) AMS sample collection from 2–4 cm depth interval. The white arrow denotes the direction of ice flow. (*b*) Microstructure tin placed in the till prior to extraction for the 0–4 cm depth interval from which thin section 1 (TS1) was produced. Ice flow is in the direction of the white arrow.

the till. Because the till contained no clasts >9.51 mm, AMS boxes were less prone to obstructions compared with field sampling. This process was repeated a total of five times to collect samples at five depths with the upper four layers containing 20 samples and the lowest most layer containing only 14. The upper surfaces of the emplaced boxes were approximately 0, 2, 4, 6, and 8 cm below the ice–bed interface. AMS samples were then sealed in plastic wrap and stored in a refrigerator to minimize desiccation until the samples were analyzed.

We measured the AMS of our samples using an AGICO Kappabridge KLS-3 magnetic susceptibility meter at the University of Wisconsin-Madison. The Kappabridge created an applied magnetic field, H, and the sample reacted by producing a unique induced magnetic field, M, where $M = kH$. Here, k is the susceptibility constant (Tarling and Hrouda 1993). The k was determined by measuring the induced magnetization of a given sample, ignoring any remnant magnetization. Samples were manually placed in three mutually perpendicular orientations and automatically rotated through 15 different orientations in the applied magnetic field. Samples showing large error (>2%) in any principal axis direction were not included in this dataset, as they were disrupted and not representative of the bulk sample. In total, two samples were discarded from the dataset. The resulting dataset can be extrapolated to find the principal magnetic susceptibility axes. When anisotropic k can be represented using an ellipsoid with long, intermediate, and short axes that are proportional to the principal susceptibility orientations, k_1, k_2, and k_3, respectively. AMS data were automatically averaged over the sample volume, reducing the significance of single-grain differences, to give the bulk anisotropy of the sample. Eigenvalues and eigenvectors were calculated for k using Steronet 11 following procedures of Mark (1973). Eigenvectors represent the directionality of the susceptibility tensors, whereas eigenvalues, S, represented the lengths of the same tensor. We collected the Horicon till used in this experiment from the exact location sourced by

Fig. 6. Thin section orientation. Thin section 1 (TS1) is oriented parallel to ice flow and spans the upper 4 cm of the till, whereas thin section 2 (TS2) is also oriented parallel to ice flow and captures 4–8 cm below the ice–till interface.

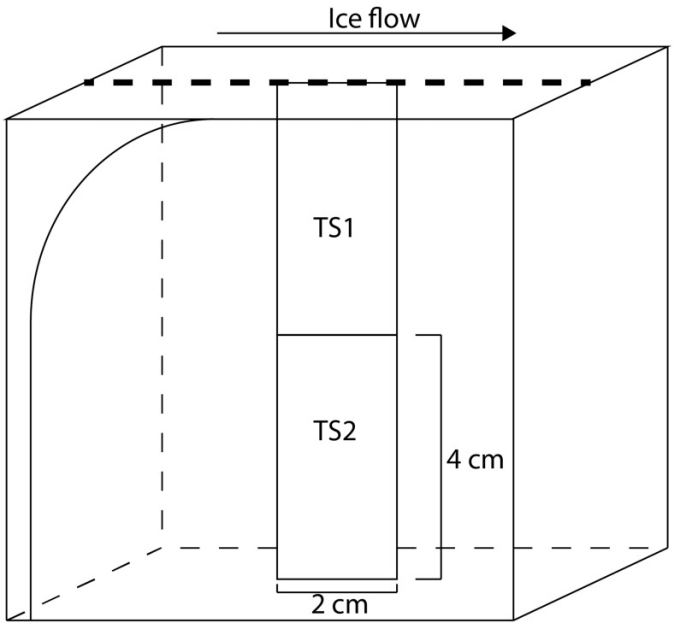

Vreeland et al. (2015); therefore, we assume the magnetic carrying mineral is magnetite as they determined.

2.3. Microstructural analysis

We also collected samples of the till following the experiment to produce sedimentological thin sections for microstructure analysis. Tin boxes, sized 4 cm × 5 cm × 9.5 cm, were pressed vertically into the bed near the centerline (Fig. 5*b*). Till around the box was gently removed, and the box was extracted. This process was repeated twice with one sample collected at ∼0–4 cm depth and a second sample collected at ∼4–8 cm depth. The long axis of the sample tin was oriented parallel to the mean ice flow direction, and the top, bottom, and sense of shear were recorded on the box. Lastly, the tins were capped, wrapped in plastic, and stored in a refrigerator until they were prepared as thin sections.

To create the thin sections, we followed the methods outlined by Rice et al. (2014). To remove water from the pore spaces in preparation for the epoxy, the tins were placed in an acetone decanter, so that acetone slowly replaced the water in the pore volume. The acetone was cycled every ∼4 days and after ∼30 days of cycling, we assumed the porewater had been replaced by the acetone and removed the sample from the decanter. At this point, Spurr's Low Viscosity Embedding Media Kit epoxy compound was added to the sample. Once the epoxy penetrated the sediment pore space, the sample was cured in the oven for 24 h. Hardened samples were cut and ground down to 30 μm thickness. The thin sections were cut vertically (2 cm × 4 cm) and oriented parallel to the ice flow direction (Fig. 6). The two thin sections presented here were effectively stacked atop each other, representing a continuous profile of deformation extending from the ice–bed interface to a depth of ∼8 cm (Fig. 6). The thin sections were then photographed on a petrographic microscope (Zeiss® Axio Imager.M2m) digital imaging device. Composite images of thin sections were compiled, and subsequently, microstructures were annotated at 6.3× magnification in plane polarized light (after Rice et al. 2019). Numerous images were taken of each thin section and stitched together using the imaging software to create a composite mosaic for each thin section. Each composite image was then mapped using CorelDraw20®.

Sediments in thin section can be subdivided into two major component parts: (i) particles <30 μm in size (or less than the thickness of the thin-section sediment slice) termed matrix (what has in the past been termed groundmass or matrix), and (ii) particles >30 μm in size termed skeleton grains or components (Fig. 2). A further group, a combined arrangement of matrix and grains, is termed S-matrix, with recognizable sets of microstructures. Matrix fabrics are illustrative of clay particle orientation within matrix, under various levels of strain, and they range from very strong orientation (unistrial) to random orientation (omnisepic) and are symptomatic of ductile deformation of clay-sized particles that compose the matrix. The S-matrix microstructures are subdivided into those which illustrate the dominance of (i) ductile, (ii) brittle, and/or (iii) polyphase (ductile and brittle, one overprinted on the other) styles of deformation, and those structures clearly indicative of porewater-induced forms due to the influence, or impact of porewater pressures, and/or porewater disruption to the surrounding sediment (Fig. 2). Many, if not all, of these microstructures can be observed within tills. Only the number and size of structures may vary from type to type.

Thin-section microstructure was analyzed using standard techniques but, importantly, the interpretations of the thin sections were conducted by a subset of the study group (e.g., Menzies) who did not conduct the experiment and from whom the deformation profile knowledge was withheld to avoid biasing the interpretation. High-resolution images were imported into a graphics software package and each microstructure type was identified and digitized into CorelDraw20®. Then, upon examination of the thin section, a detailed microfabric-microstructural "map" of the thin section was produced (Phillips et al. 2011; van der Meer and Menzies 2011) like those seen in Fig. 2. Consequently, a large dataset of individual microstructure types including size and orientation (fabric) can be obtained from either the whole, or key parts of the thin section. These data establish the spatial distribution and relationships between microstructures and microstructure fabrics.

3. Results

During this experiment, we implemented a range of effective pressures (8–113 kPa) and slip speeds (25–300 m/yr) over a period of ∼9 days for a total ice displacement of ∼3.72 m at the outer boundary (Table 1). Overall, the total displacement within the most deformed zone (upper ∼2 cm of the till) equated to a shear strain of approximately 316 (see Table 1) (Fig. 7*a*). The deflection of the strain markers in the till bed

Fig. 7. Strain estimation. (*a*) Displacement results from DIC velocimetry in the upper layer (~4 cm) of the till. (*b*) Displacement of beads that were originally vertical. Photo spans from the ice–till interface (at the top of the photo) down to ~10 cm depth. Ice flow was from left to right as indicated by the black arrow. Each box on the scale is 1 cm. The displacement in the upper ~2.5 cm is great enough that the beads have been advected out of the image. The green boxes in (*a*) and (*b*) span the same zone, but the horizontal axis' scale is vastly different. (*c*) Strain estimates for the entire deforming zone estimated from (*a*) and (*b*) binned into 2 cm layers.

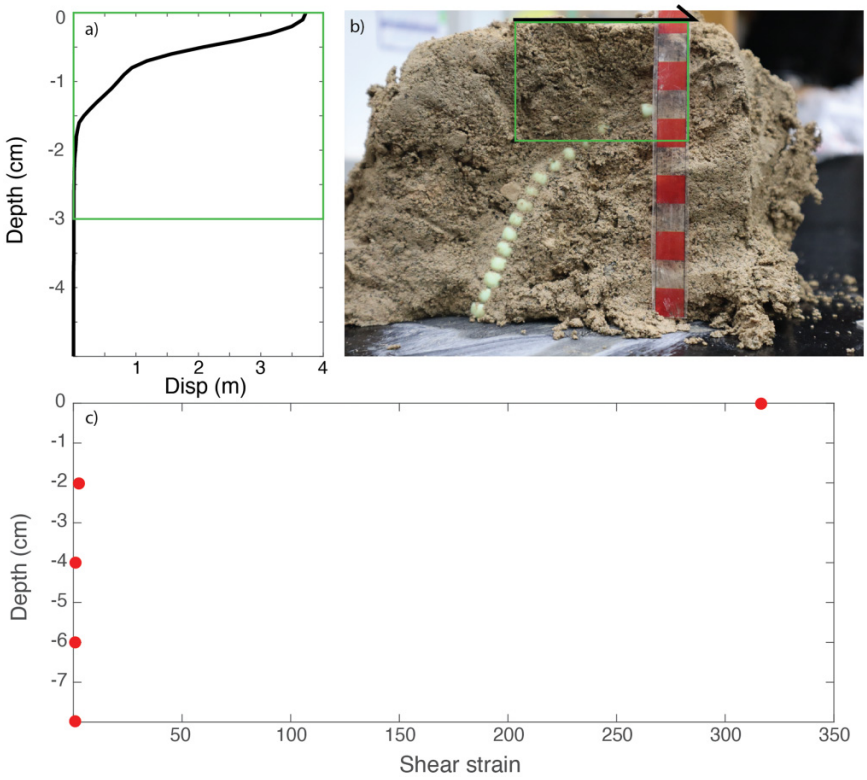

indicates that shear strain greater than 1 extended to a depth of ~6 cm below the ice–bed interface (Fig. 7*b*). We bin strain results from the DIC and the beads into 2 cm thick layers (the size of the AMS boxes) spanning the thickness of the bed and estimate shear strains for each bin (Fig. 7*c*). The absence of beads in the top layer of the till column shown in Fig. 7*b* results from large strain (>>10) in that region where the beads were advected out of the photo's field of view. For the upper ~2 cm where strain was very high, we estimate shear strain from the DIC measurements shown in Table 1 and Fig. 7*a*. In the bottom ~8 cm where strain was smaller, we estimate shear strain directly from the beads (Fig. 7*b*). The strain profile in the bottom 8 cm of the bed has a concave down profile (Fig. 7), and the thickness of the highly deformed zone is ~40 times the median grain size, D_{50} ~ 0.530 mm (Fig. 4). Shear strains greater than ~10 are sufficient to develop steady-state fabric and microstructure (Iverson et al. 2008).

Likewise, AMS data show that deformation is pronounced in the upper 2 cm of the till, but the degree of fabric development decreases substantially with depth (Figs. 8 and 9; Table 2). In the upper 2 cm of the till, the k_1 eigenvector azimuth (~190°) generally aligns with the ice flow azimuth (N-S) and has an apparent up ice-plunge of 21° (Fig. 8*a*). This top layer (0–2 cm) is contained entirely within the highly deformed zone, and the S_1 eigenvalue is large (S_1 = 0.94) indicating a high degree of clustering around a central vector. As depth increases, the amount of strain and corresponding S_1 eigenvalue decreases (Fig. 8; Table 2). Between depths of 2 and 6 cm, eigenvalues are of medium strength (S_1 = 0.74 and S_1 = 0.70 for depth intervals of 2–4 cm and 4–6 cm, respectively); however, differences in their k_1 azimuth indicate different degrees of deformation. At 2–4 cm depth (Fig. 8*b*), deformation is generally aligned with the k_1 azimuth (188.9°) with the ice flow direction (N-S), whereas at the 4–6 cm depth, the k_1 azimuth (158.8°) begins to vary from the ice flow direction (N-S) (Fig. 8*c*). In the bottom 6–10 cm of the till (Figs. 8*d* and 8*e*), eigenvalues are low (S_1 = 0.57 and S_1 = 0.51), and eigenvector orientation does not align with the ice flow direction (also see Table 2). This indicates that deformation in that zone was insufficient to align the particles, which generally agrees with the observed deflection of the beads (shear strains <0.5). The apparent plunge in the upper highly deformed zone (21°) from the shear plane has been observed in other laboratory studies, which they attribute to the formation of Riedel shear planes developing in the deformed zone (Iverson et al. 2008).

The distribution of microstructures observed in both thin sections (Figs. 10*a* and 10*b*) suggests localized shear strain and a shear stress that generally falls below the tills shear strength at depth. Both thin sections lack discrete porewater

Fig. 8. AMS results. Lower hemisphere stereo plots with ice flow direction (N-S). The eigenvalues of the k_1 (max), k_2 (int), and k_3 (min) are shown for each depth interval. The points cluster more tightly in the highly deformed till near the ice–bed interface (0–2 cm) and begin to decrease with depth. Arrows in lower right indicate sense of shear.

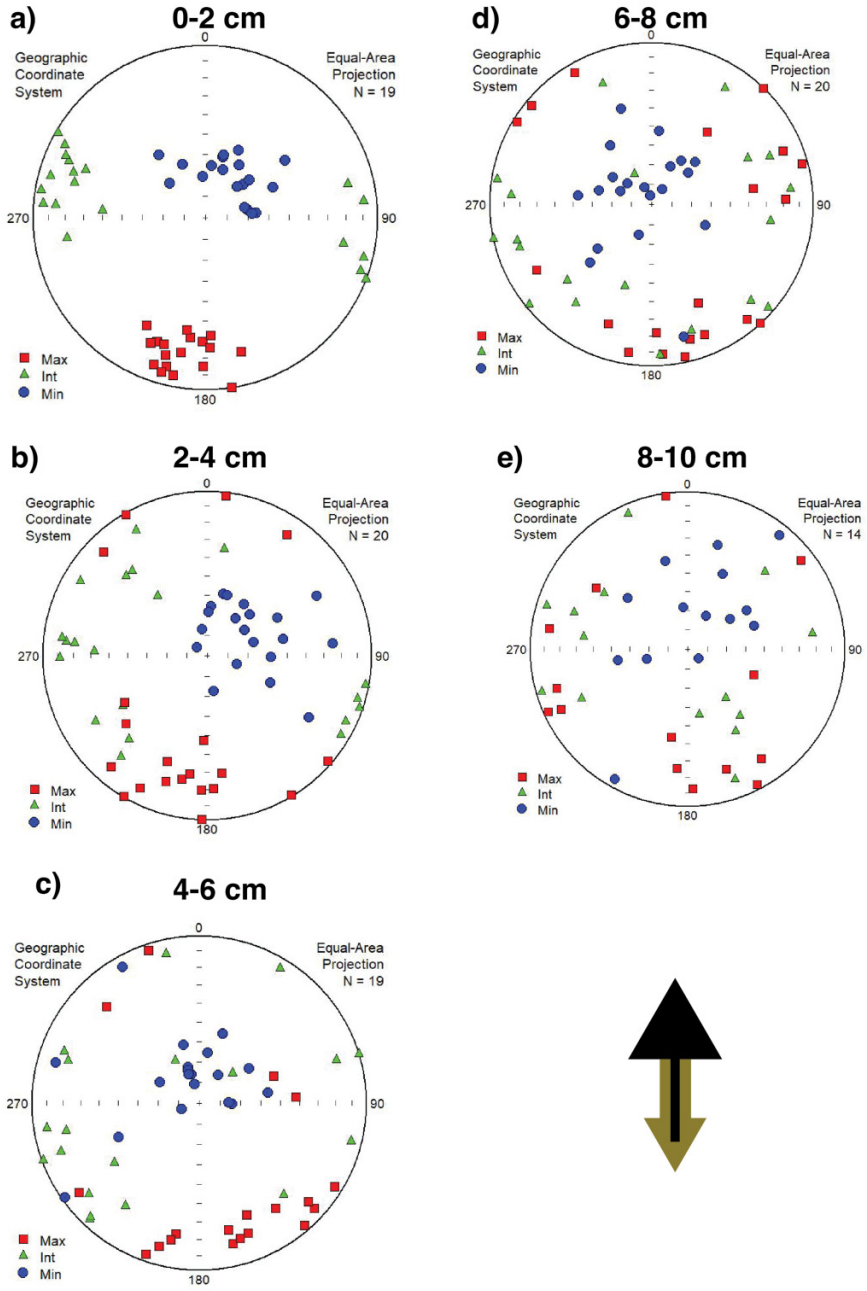

passageways, such as water escape structures, nondiscrete clay cutans, or open void spaces (see Figs. S1 and S2 for these and additional microstructures). The upper thin section (~0–4 cm depth), hereafter denoted TS1 (Fig. 10*c*), is clast-rich with many subangular and subrounded small grains and few large clasts. There are no substantial clast-free areas of matrix, and no domains are present. Domains are recognized in thin section images as areas of differing grain size, clay content, or color, or having a distinct subfacies property (e.g., clast content and angularity, clay matrix, etc.) (Menzies and van der Meer 2018, p. 768). Domains in thin sections occur as aggregations of fine-grained (clay) particles slipping under compressive stress; as reorientated aggregates within failure zones (deformation shear zones and/or bands); or as cutans (argillans) deposited in dilated pore spaces. Domains are often overprinted by later structures and may have an impact on the orientation and reorientation of subsequent formation of other microstructures. Clasts are relatively evenly distributed throughout the sediment, indicating it was homogenized during transport and emplacement (Fig. 10). In addition, we identify less than five edge-to-edge grain crushing events at grain contacts (edge-to-edge) (Fig. S1), which may indicate either (i) low effective pressure leading to few grains "touching", or (ii) fine grains cushioning larger grains.

Fig. 9. Strain versus S_1 eigenvalue. S_1 eigenvalues increase rapidly with strain but level off around 0.9. For comparison, the eigenvalues from Iverson et al. (2008) are also shown, which were also completed on the Horicon till but without the presence of ice.

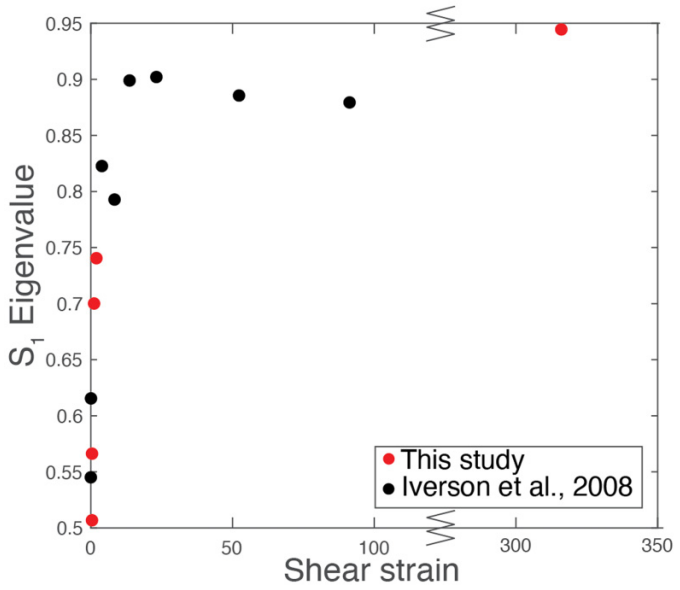

Grain stacks are common throughout TS1 with a slightly higher concentration in the central portion of the slide (Fig. 10; Figs. S1 and S2). Their dominant orientation is subvertical and orthogonal to the prevailing microshear direction. As grain stacks are often indicative of early stages of pervasive deformation, it is likely clasts readjusted in the till when vertical stress was first applied, inducing deformative flow in a near vertical manner. Microshears are more prevalent, especially in the upper part of TS1 (Fig. 10), and their fabrics exhibit a bimodal distribution. The dominant microshears (denoted with a light pink stress zone in Fig. 10*c*) stretch from upper left to lower right consistent with R1-type Riedel shears. The second population of microshears (unshaded in Fig. 10*c*) tend to stretch from lower left to upper right in accordance with an R2-type Riedel shear. It is possible that these two groups of microshears indicate separate phases of shearing (Gehrmann et al. 2017) or that they represent R1 and R2 Riedel shears. Rotation structures appear distributed randomly throughout the thin section, though they typically occur around larger clasts (see Figs. S1 and S2). Collectively, the microstructures identified in TS1 indicate principal stresses passed from the upper surface of the till bed from left to right. It might be further surmised that effective pressure was low since the stress dissipation seems rapid into the underlying sediment pile with few edge-to-edge grain crushing events.

The lower thin section, TS2 (Fig. 10*d*), is also clast-rich but contains several domains that are slightly coarser than the surrounding sediment and likely incorporated prior to deformation. Both grain stacks and microshears exhibit a joint, subvertical, parallelism. The microshears here (Fig. 10*d*) are steeply angled and have a stronger preferred orientation than in TS1 (Fig. 10*c*). These are possible R2-type shears due to stress diminution with depth within the sediment. The domains here are intact and behave as a cohesive unit that will experience progressive rounding due to transport. As the domains are largely subrounded in TS2, they indicate a lack of transport under stress compared with TS1 and thus reduced homogenization under shear strain deformation.

4. Discussion and conclusions

Overall, the vast majority of shear strain in the till occurred in the ~2.5 cm of the bed near the ice–bed interface, but small amounts of deformation extended through the full depth (Fig. 7). In total, till flux through the upper ~2.5 cm where pervasive deformation occurred was approximately 20-fold greater than the deeper portion of the bed (Fig. 7). Though beads recorded small strain between depths of 4 and 10 cm, AMS was not particularly diagnostic at this low level (Table 1). Strain at the lower depths contributes minimally to ice flow; however, it is possible over extended periods of time that tills could become sufficiently deformed to exhibit well aligned fabrics and critical state porosities. For example, we measure a shear strain of ~0.40 for the bottom 2 cm of the bed, which accumulated over ~9 days. If the conditions of the experiment were to persist for ~1 year, this bottom layer till could hypothetically reach a shear strain of ~10. This would produce well-defined fabrics and a critical state porosity, all without ever deforming rapidly. This could explain why zones of deep deformation (several meters) have been inferred from active source seismic analysis of basal Antarctic tills (Blankenship et al. 1986), while borehole observations from those same ice streams (Kamb 2001) have shown that slip facilitating strain typically localizes in a zone near the ice–bed interface on the order of 10^0–10^1 cm deep.

In general, our AMS results replicate observations from previous ice-free deformation experiments that used a split-cell ring shear device with the same Horicon till (Iverson et al. 2008; Vreeland et al. 2015). This agreement indicates those results are robust in their application to shear induced by ice slippage (Fig. 9). Maximum S_1 eigenvalues ($S_1 = 0.90$) reported by Iverson et al. (2008) were slightly lower than ours ($S_1 = 0.94$). Furthermore, Vreeland et al. (2015) reported an up-ice plunge of 28° in highly deformed Horicon till, whereas we record a 21° up-ice plunge. The ~7° difference here is generally small compared with the full range of possible plunges; nonetheless, the influence of the ice could be responsible for this small variation. The flow of meltwater through the upper layer of the till near the ice sole may elevate porewater pressures to the point where local shear strength is further decreased relative to till deeper in the bed (Tulaczyk et al. 2000*a*). However, the greater degree of mobility does not appear to significantly affect the steady-state fabrics and microstructures that develop in the till. This likely stems from the observation that fabric reaches its maximum S_1 eigenvalue beyond strains of ~10 (Iverson et al. 2008), reflecting a balance between many competing factors that work to set the overall structure of the deforming zone. Though water flow induced by ice melt may enhance the mobility of sediment near the ice–bed interface, this simply causes the till

Table 2. AMS results.

Sample depth (cm)	Number of samples	k	Eigenvalue, S	Eigenvector azimuth (°)	Eigenvector plunge (°)	Shear strain
0–2	19	k_1	0.94	190.4	21.1	316
0–2	19	k_2	0.90	282.9	7.7	316
0–2	19	k_3	0.91	31.9	67.4	316
2–4	20	k_1	0.74	188.9	17.5	1.98
2–4	20	k_2	0.70	283.8	17.7	1.98
2–4	20	k_3	0.83	60.3	66.0	1.98
4–6	19	k_1	0.70	158.8	15.5	1.17
4–6	19	k_2	0.64	248.7	9.2	1.17
4–6	19	k_3	0.75	0.5	75.8	1.17
6–8	20	k_1	0.57	158.5	10.9	0.43
6–8	20	k_2	0.54	254.0	1.1	0.43
6–8	20	k_3	0.77	330.2	78.3	0.43
8–10	14	k_1	0.51	175.9	17.7	0.42
8–10	14	k_2	0.47	114.3	5.5	0.42
8–10	14	k_3	0.68	17.9	62.5	0.42

to reach the steady-state fabric sooner provided the forcing conditions do not change (e.g., effective pressure, ice flow direction). In effect, our results indicate that the complexity of the cryogenic ring shear is not required to accurately assess fabric development in sandy subglacial tills and that, to a first order, split-cell sediment ring shear devices suffice for this analysis. Two areas that warrant further examination are the effects of a suprajacent ice layer (i) on deformation structures in fine-grained, clay-rich tills and (ii) in the matrix around ploughing clasts. Different mechanics may operate in the till matrix of fine-grained, matrix-supported tills (in contrast with the sandy Horicon till tested here). Their general reduction in permeability may cause even greater elevation of pore pressures near the ice–bed interface. Such an effect could cause shallower deformation or potentially decouple the ice from the bed reducing deformation within the till. Similarly, large ploughing structures at the ice–bed interface drive deformation deeper in till (Tulaczyk et al. 2001; Zoet and Iverson 2020), which may produce a range of diagnostic fabrics and microstructures in the lee of the ploughing obstacle.

Throughout both thin sections, we identified a variety of microstructures, with microshears, grain stacks, and rotational structures being the dominant forms. Notably, they point to an initial rheological phase change from pervasive deformation (likely under vertical loading) to localized strain during shear, such that several generations of microstructures appear in the mapped thin sections. In the upper portion of the TS1 (depth ~0–3 cm), microshears are colocated with a region of high strain, and their dominant orientation (~18° from horizontal) agrees with the expected orientation of Riedel shears (Fig. 10*c*). Additionally, the observed orientations of the R1- and R2-type shears may give rise to the 21° up-ice plunge of the grains that we resolved through AMS in the upper 2 cm of the till (Thomason and Iverson 2006; see their figure 7). In the lower 5 cm of the thin sections (i.e., ~3–8 cm depth in the bed), some microshears are present but plunge at a much steeper angle, ~60° and ~120° from horizontal in the direction of ice flow (Fig. 10*d*). We hypothesize these features developed during the initial loading and consolidation phase of our experiment. During this process, the till bed experiences pure shear that could hypothetically produce steeply dipping microshears that would subsequently be erased in zones of large deformation (i.e., the top ~2.5 cm of the bed). Rotational structures populated both thin sections, even in zones of minimal (but nonzero) strain (Table 2). The presence of subrounded domains (due to transport as noted above) in the lower 4 cm of the thin sections also indicates minimal strain. Microshears therefore appear to be better diagnostic indicators of high total strain, whereas rotational structures seem to represent some finite amount of strain that can be quite low. It is worth noting that grain stacks develop under pervasive shear, as opposed to microshears and rotation structures that form once the sediment focuses shear localization that results in nonpervasive deformation. These thin sections were interpreted initially without any knowledge of the strain accumulation, and the inferred dynamics agree well with the known history of the till and distribution of shear strain (Fig. 7). This analysis emphasizes that in the correct hands, microstructure analysis is a valuable diagnostic tool for highly deformed tills.

These results serve as a baseline for comparison with in-situ tills. In many ways, they should be viewed as a "best case scenario" for natural tills, since many complexities encountered in nature were either precisely controlled and/or measured in these experiments. This level of monitoring is obviously not possible in the natural world, so caution would be wise in interpreting natural samples beyond the level of detail captured in this study since available information may be insufficient to resolve very fine details.

In summary, we find that highly deformed till is confined to a narrow band near the ice–bed interface but small amounts of shear strain extend deeper into the till bed. These deeper zones likely do little to regulate glacier drag

Fig. 10. Thin sections. Microstructures of TS1 and TS2. Ice flow is from left to right in all images: (*a*) TS1 from 0–4 cm depth, (*b*) TS2 from 4–8 cm depth, and (*c*) TS1 microstructures. The microshears (shown in blue) are dipping down ice as R1 shears, while a few high-angle microshears are dipping up ice, which may be R2 shears. (*d*) TS2 samples from a depth of 4–8 cm below the ice–till interface in the zone where the till deformation was minimal. The R1 shears found in TS1 are largely absent but the high-angle shear structures persist. The high-angle microshears in TS2 could be the result of pure shear imposed from the initial consolidation of the till.

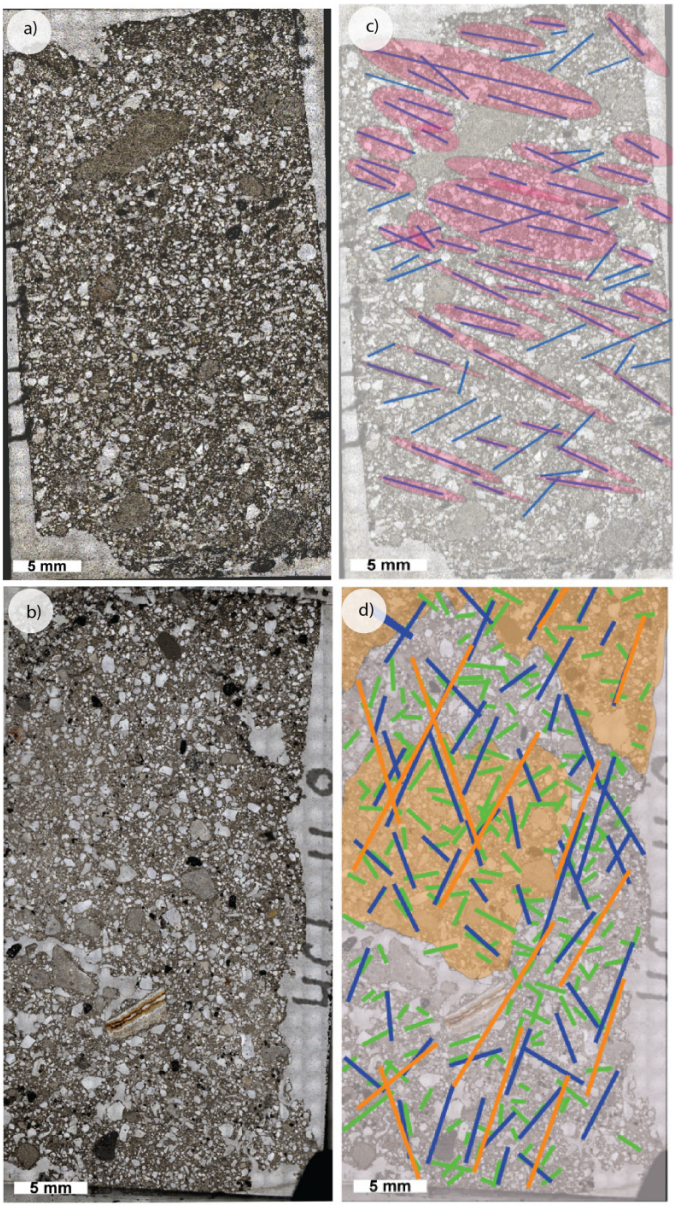

and advect relatively small volumes of till. However, with adequate time, it is possible that sufficient strain could accumulate within them as to appear highly deformed. AMS results show high eigenvalues in zones of extensive deformation (upper ~2 cm), with eigenvectors oriented in the direction of ice flow. These findings are consistent with behavior previously observed in split-cell sediment ring shear devices. Furthermore, microstructures (especially microshears) are abundant in zones of high deformation, and their orientations generally align with the plunge of particles measured by AMS. Till flux through the highly deformed upper ~2.5 cm of the bed is approximately 20-fold greater than the deeper portion—emphasizing that controls on deformation in this upper zone are of central importance for landform construction and erosion (Hansen and Zoet 2022). Lastly, since the properties of this narrow deformation zone heavily influence glacier slip (Zoet and Iverson 2020), identifying and examining them in the geologic record is critical to constraining glacier flow mechanics. The current study describes the kinematics within the highly deformed zone, providing a reasonable set of characteristics that can be used as diagnostic indicators.

Acknowledgements

Thanks to Drae Rodgers for preparing the thin sections, and Mike Spicuzza and Lillian Smith for their help in photographing the thin sections. We thank Jeremy Ely and Jason Thomason for thoughtful reviews that improved the manuscript.

Article information

History dates

Received: 5 July 2022
Accepted: 12 December 2022
Accepted manuscript online: 9 January 2023
Version of record online: 16 February 2023

Copyright

Data availability

Experimental data are archived at https://minds.wisconsin.edu/handle/1793/82882 and thin section and AMS data are available at http://digital.library.wisc.edu/1793/83771.

Author information

Author ORCIDs

L.K. Zoet https://orcid.org/0000-0002-9635-4051
D.D. Hansen https://orcid.org/0000-0002-9150-9376
J. Menzies https://orcid.org/0000-0001-5446-3025

Author notes

This article is part of a collection titled "GAC-MAC Glacial Session".

Author contributions

Conceptualization: LKZ
Data curation: LKZ
Formal analysis: LKZ, DDH, NMW
Funding acquisition: LKZ
Investigation: LKZ, DDH, JM
Methodology: LKZ
Project administration: LKZ

Resources: PS, NL
Supervision: LKZ
Visualization: JM
Writing – original draft: LKZ
Writing – review & editing: LKZ, DDH, NMW, JM

Competing interests

The authors declare that there are no competing interests.

Funding information

This work was supported by NSF Award OPP 2013987 to LKZ.

Supplementary material

Supplementary data are available with the article at https://doi.org/10.1139/CJES-2022-0074.

References

Alley, R.B., Blankenship, D.D., Bentley, C.R., and Rooney, S.T. 1986. Deformation of till beneath ice stream B, West Antarctica. Nature, **322**: 57–59. Nature Publishing Group. doi:10.1038/322057a0.

Anandakrishnan, S., and Alley, R.B. 1994. Ice stream C, Antarctica, sticky spots detected by microearthquake monitoring. Annals of Glaciology, **20**: 183–186. Cambridge University Press. doi:10.3189/1994AoG20-1-183-186.

Ankerstjerne, S., Iverson, N.R., and Lagroix, F. 2015. Origin of a washboard moraine of the Des Moines Lobe inferred from sediment properties. Geomorphology, **248**: 452–463. doi:10.1016/j.geomorph.2015.07.019.

Bart, P.J., and Tulaczyk, S. 2020. A significant acceleration of ice volume discharge preceded a major retreat of a West Antarctic paleo–ice stream. Geology, **48**: 313–317. doi:10.1130/G46916.1.

Benn, D.I., and Evans, D.J. 2010. Glaciers & glaciation. Routledge.

Blankenship, D.D., Bentley, C.R., Rooney, S.T., and Alley, R.B. 1986. Seismic measurements reveal a saturated porous layer beneath an active Antarctic ice stream. Nature, **322**: 54–57. Nature Publishing Group. doi:10.1038/322054a0.

Boulton, G.S. 1986. Geophysics: a paradigm shift in glaciology? Nature, **322**: 18. Nature Publishing Group. doi:10.1038/322018a0.

Clark, C.D. 1993. Mega-scale glacial lineations and cross-cutting ice-flow landforms. Earth Surface Processes and Landforms, **18**: 1–29. doi:10.1002/esp.3290180102.

Colgan, P.M., Mickelson, D., and Cutler, P. 2003. Ice-marginal terrestrial landsystems: southern Laurentide Ice Sheet margin. *In* Glacial Landsystems. pp. 1–32.

Colman, S., Breckenridge, A., Zoet, L.K., Wattrus, N., and Johnson, T.C. 2020. Moraines and late-glacial stratigraphy in central Lake Superior. Quaternary Research, **98**: 19. doi:10.1017/qua.2020.36.

Creyts, T.T., and Schoof, C. 2009. Drainage through subglacial water sheets. Journal of Geophysical Research, **114**: F04008. doi:10.1029/2008JF001215.

Damsgaard, A., Egholm, D.L., Piotrowski, J.A., Tulaczyk, S., Larsen, N.K., and Tylmann, K. 2013. Discrete element modeling of subglacial sediment deformation. Journal of Geophysical Research, Earth Surface, **118**: 2230–2242. doi:10.1002/2013JF002830.

Damsgaard, A., Goren, L., and Suckale, J. 2020. Water pressure fluctuations control variability in sediment flux and slip dynamics beneath glaciers and ice streams. Communications Earth & Environment, **1**: 1–8. Nature Publishing Group. doi:10.1038/s43247-020-00074-7.

Gehrmann, A., Hüneke, H., Meschede, M., and Phillips, E. 2017. 3D microstructural architecture of deformed glacigenic sediments associated with large-scale glacitectonism, Jasmund Peninsula (NE Rügen), Germany. Journal of Quaternary Science, **32**: 213–230. doi:10.1002/jqs.2843.

Gentoso, M.J., Evenson, E.B., Kodama, K.P., Iverson, N.R., Alley, R.B., Berti, C., and Kozlowski, A. 2012. Exploring till bed kinematics using AMS magnetic fabrics and pebble fabrics: the Weedsport drumlin field, New York State, USA. Boreas, **41**: 31–41. doi:10.1111/j.1502-3885.2011.00221.x.

Hansen, D.D., and Zoet, L.K. 2022. Characterizing sediment flux of deforming glacier beds. JGR Earth Surface, **127**: e2021JF006544. doi:10.1029/2021JF006544.

Hart, J.K., Rose, K.C., Martinez, K., and Ong, R. 2009. Subglacial clast behaviour and its implication for till fabric development: new results derived from wireless subglacial probe experiments. Quaternary Science Reviews, **28**: 597–607. doi:10.1016/j.quascirev.2008.07.020.

Head, K.H. 1989. Soil technician's handbook. John Wiley and Sons, New York, NY.

Hiemstra, J., and Rijsdijk, K. 2003. Observing artificially induced strain: implications for subglacial deformation. Journal of Quaternary Science, **18**: 373–383. doi:10.1002/jqs.769.

Hooyer, T.S., Iverson, N.R., Lagroix, F., and Thomason, J.F. 2008. Magnetic fabric of sheared till: a strain indicator for evaluating the bed deformation model of glacier flow. Journal of Geophysical Research, **113**. doi:10.1029/2007JF000757.

Iverson, N.R. 2017. Determining glacier flow direction from till fabrics. Geomorphology, **299**: 124–130. doi:10.1016/j.geomorph.2017.10.005.

Iverson, N.R., Hooyer, T.S., and Baker, R.W. 1998. Ring-shear studies of till deformation: Coulomb-plastic behavior and distributed strain in glacier beds. Journal of Glaciology, **44**: 634–642. Cambridge University Press. doi:10.3189/S0022143000002136.

Iverson, N.R., Hooyer, T.S., Thomason, J.F., Graesch, M., and Shumway, J.R. 2008. The experimental basis for interpreting particle and magnetic fabrics of sheared till. Earth Surface Processes and Landforms, **33**: 627–645. doi:10.1002/esp.1666.

Ives, L.R.W., and Iverson, N.R. 2019. Genesis of glacial flutes inferred from observations at Múlajökull, Iceland. Geology, **47**: 387–390. doi:10.1130/G45714.1.

Jacobson, W.R., and Hooyer, T.S. 2015. Laboratory study of fabric development in shearing till: the importance of effective pressure and shearing rate. Geomorphology, **250**: 249–257. doi:10.1016/j.geomorph.2015.08.008.

Kamb, B. 2001. Basal zone of the West Antarctic ice streams and its role in lubrication of their rapid motion. *In* The West Antarctic Ice Sheet: behavior and environment. American Geophysical Union (AGU). pp. 157–199. doi:10.1029/AR077p0157.

Kasmalkar, I., Damsgaard, A., Goren, L., and Suckale, J. 2021. Shear variation at the ice–till interface changes the spatial distribution of till porosity and meltwater drainage. JGR Earth Surface, **126**: e2021JF006460. doi:10.1029/2021JF006460.

Larson, G.J., Lawson, D.E., Evenson, E.B., Alley, R.B., Knudsen, Ó., Lachniet, M.S., and Goetz, S.L. 2006. Glaciohydraulic supercooling in former ice sheets? Geomorphology, **75**: 20–32. doi:10.1016/j.geomorph.2004.12.009.

Mark, D.M., 1973. Analysis of axial orientation data, including till fabrics. Geological Society of America Bulletin, **84**: 1369–1374. doi:10.1130/0016-7606(1973)84%3c1369:AOAODI%3e2.0.CO;2.

McCracken, R.G., Iverson, N.R., Benediktsson, Í.Ö., Schomacker, A., Zoet, L.K., Johnson, M.D., et al. 2016. Origin of the active drumlin field at Múlajökull, Iceland: new insights from till shear and consolidation patterns. Quaternary Science Reviews, **148**: 243–260. doi:10.1016/j.quascirev.2016.07.008.

Menzies, J. 2000. Microstructures in diamictites of the lower Gowganda Formation (Huronian), near Elliot Lake, Ontario: evidence for deforming-bed conditions at the grounding line? Journal of Sedimentary Research, **70**: 210–216. doi:10.1306/2DC4090B-0E47-11D7-8643000102C1865D.

Menzies, J. 2000a. Microstructures in diamictites of the lower Gowganda Formation (Huronian), near Elliot Lake, Ontario: evidence for deforming-bed conditions at the grounding line?. Journal of Sedimentary Research, **70**(1): 210–216. doi:10.1306/2DC4090B-0E47-11D7-8643000102C1865D.

Menzies, J. 2000b. Micromorphological analyses of microfabrics and microstructures indicative of deformation processes in glacial sediments. Geological Society, London, Special Publications, **176**(1): 245–257. doi:10.1144/GSL.SP.2000.176.01.19.

Menzies, J., and Meer, J.J. 2018. Micromorphology and microsedimentology of glacial sediments. Past glacial environments, 753–806. Elsevier. doi:10.1016/B978-0-08-100524-8.00036-1.

Menzies, J., Hess, D.P., Rice, J.M., Wagner, K.G., and Ravier, E. 2016. A case study in the New York Drumlin Field, an investigation using microsedimentology, resulting in the refinement of a theory of drumlin formation. Sedimentary Geology, **338**: 84–96. doi:10.1016/j.sedgeo.2016.01.017.

Menzies, J., Zaniewski, K., and Dreger, D. 1997. Evidence, from microstructures, of deformable bed conditions within drumlins, Chimney Bluffs, New York State. Sedimentary Geology, **111**: 161–175. doi:10.1016/S0037-0738(97)00013-4.

Mickelson, D.M., and Syverson, K.M. 1997. Quaternary geology of Ozaukee and Washington counties, Wisconsin - Quaternary geology of Ozaukee and Washington counties, Wisconsin - WGNHS. Wisconsin Geological and Natural History Survey Bulletin, **91**.

Müller, B.U., and Schlüchter, C. 2000. Influence of the glacier bed lithology on the formation of a subglacial till sequence: ring-shear experiments as a tool for the classification of subglacial tills. Quaternary Science Reviews, **20**: 1113–1125. doi:10.1016/S0277-3791(00)00141-4.

Phillips, E., van der Meer, J.J.M., and Ferguson, A. 2011. A new "microstructural mapping" methodology for the identification, analysis and interpretation of polyphase deformation within subglacial sediments. Quaternary Science Reviews, **30**: 2570–2596. doi:10.1016/j.quascirev.2011.04.024.

Piotrowski, J.A., Mickelson, D.M., Krzyszkowski, D., and Junge, F.W. 2001. Were deforming subglacial beds beneath past ice sheets really widespread? Quaternary International.

Ravier, E. 2014 Structures de déformation induites par surpressions de fluide dans les environnements sous-glaciaires et marin profonds: implications paléoenvironnementales et réservoirs University de Bourgogne (Doctoral dissertation, Dijon). 526 pp.

Rice, J., Paulen, R., Menzies, J., and McClenaghan, M.B. 2014. Micromorphological descriptions of till from pit K-62, Pine Point mining district, Northwest Territories, Report number: Geological Survey Of Canada Open File 7526. doi:10.4095/293478.

Rice, J.M., Menzies, J., Paulen, R.C., and McClenaghan, M.B. 2019. Microsedimentological evidence of vertical fluctuations in subglacial stress from the northwest sector of the Laurentide Ice Sheet, Northwest Territories, Canadian Journal of Earth Sciences, **56**: 363–379. NRC Research Press. doi:10.1139/cjes-2018-0201.

Shumway, J.R., and Iverson, N.R. 2009. Magnetic fabrics of the Douglas Till of the Superior lobe: exploring bed-deformation kinematics. Quaternary Science Reviews, **28**: 107–119. doi:10.1016/j.quascirev.2008.09.020.

Spagnolo, M., Phillips, E., Piotrowski, J.A., Rea, B.R., Clark, C.D., Stokes, C.R., et al., 2016. Ice stream motion facilitated by a shallow-deforming and accreting bed. Nature Communications, **7**(1): 1–11. doi:10.1038/ncomms10723.

Stanford, S.D., and Mickelson, D.M. 1985. Till fabric and deformational structures in drumlins near Waukesha, Wisconsin, U.S.A. Journal of Glaciology, **31**: 220–228. Cambridge University Press. doi:10.3189/S0022143000006535.

Tarling, D., and Hrouda, F. 1993. Magnetic anisotropy of rocks. Springer Science & Business Media.

Thomason, J., and Iverson, N. 2006. Microfabric and microshear evolution in deformed till. Quaternary Science Reviews, **25**: 1027–1038. doi:10.1016/j.quascirev.2005.09.006.

Tulaczyk, S. 1999. Ice sliding over weak, fine-grained tills: dependence of ice-till interactions on till granulometry. *In* Special Paper of the Geological Society of America. pp. 159–177. doi:10.1130/0-8137-2337-X.159.

Tulaczyk, S., Kamb, W.B., and Engelhardt, H.F. 2000a. Basal mechanics of Ice Stream B, west Antarctica: 1. Till mechanics. Journal of Geophysical Research, **105**: 463–481. doi:10.1029/1999JB900329.

Tulaczyk, S., Kamb, W.B., and Engelhardt, H.F. 2000b. Basal mechanics of Ice Stream B, west Antarctica: 2. Undrained plastic bed model. Journal of Geophysical Research, **105**: 483–494. doi:10.1029/1999JB900328.

Tulaczyk, S.M., Scherer, R.P., and Clark, C.D., 2001. A ploughing model for the origin of weak tills beneath ice streams: a qualitative treatment. Quaternary International, **86**(1): 59–70. doi:10.1016/S1040-6182(01)00050-7.

Tylmann, K. 2012. Sedimentary record of an ice/bed interface mosaic: deforming spots intervening with stable bed areas at Sampława, northern Poland. Quaternary International, **279–280**: 506. doi:10.1016/j.quaint.2012.08.1739.

van der Meer, J.J., and Menzies, J. 2011. The micromorphology of unconsolidated sediments. Sedimentary Geology, **238**(3-4): 213–232. doi:10.1016/j.sedgeo.2011.04.013.

van der Meer, J.J.M., Menzies, J., and Rose, J. 2003. Subglacial till: the deforming glacier bed. Quaternary Science Reviews, **22**: 1659–1685. doi:10.1016/S0277-3791(03)00141-0.

Vreeland, N.P., Iverson, N.R., Graesch, M., and Hooyer, T.S. 2015. Magnetic fabrics of drumlins of the Green Bay Lobe, southeastern Wisconsin. Quaternary Science Reviews, **112**: 33–44. doi:10.1016/j.quascirev.2015.01.015.

Woodard, J.B., Zoet, L.K., Benediktsson, Í.Ö., Iverson, N.R., and Finlayson, A. 2020. Insights into drumlin development from ground-penetrating radar at Múlajökull, Iceland, a surge-type glacier. Journal of Glaciology, **66**: 822–830. doi:10.1017/jog.2020.50.

Zoet, L.K., and Iverson, N.R. 2018. A healing mechanism for stick-slip of glaciers. Geology, **46**: 807–810. doi:10.1130/G45099.1.

Zoet, L.K., and Iverson, N.R. 2020. A slip law for glaciers on deformable beds. Science, **368**: 76–78. American Association for the Advancement of Science. doi:10.1126/science.aaz1183. PMID: 32241945.

Zoet, L.K., Rawling, J.E., III, Woodard, J.B., Barrette, N., and Mickelson, D.M. 2021. Factors that contribute to the elongation of drumlins beneath the Green Bay Lobe, Laurentide Ice Sheet. Earth Surface Processes and Landforms, **46**: 2540–2550. doi:10.1002/esp.5192.